THE JOURNAL OF PHYSICAL CHEMISTRY C

Article

pubs.acs.org/JPCC

Observation of Nanoparticle-Enhanced Marangoni Transport near a Freezing Out Front

Haeng Sub Wi,[†] Sreeram Cingarapu,[‡] Ken J. Klabunde,[‡] Chris M. Sorensen,[†] and Bruce M. Law*,[†]

[†]Department of Physics, Kansas State University, Manhattan, Kansas 66506, United States

[‡]Department of Chemistry, Kansas State University, Manhattan, Kansas 66506, United States

ABSTRACT: We report observation of an unusual nanoparticle (NP)-enhanced Marangoni flow near the melting point of a dodecanethiol ligated Au NP−octadecane solution. A thermal gradient (0.74 °C/cm) is applied to a thin film of this NP−octadecane mixture in an open Teflon trough parallel to the liquid−vapor surface. Half the mixture is frozen, and the other half is liquid. Over a period of many hours, thermal and solutal Marangoni flow transports the liquid in the direction of the solidified mixture where a "mountain" of this material builds up over time at the liquid−solid boundary due to the presence of this liquid flow. Small quantities of NPs in the bulk solution (NP volume fractions of ~10^{-5}) enhance this Marangoni flow by upward of factors of 4 relative to pure octadecane. We believe that this effect is due to the freezing out of NPs (relative to the liquid octadecane) within a thin liquid film that flows over the solidified NP−octadecane mixture; this freezing out of NPs within the thin film creates a large NP gradient at the liquid−vapor surface which generates an enhanced solutal Marangoni flow.

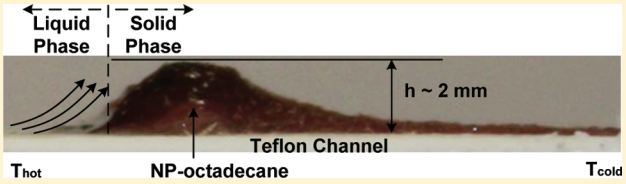

1. INTRODUCTION

The Marangoni effect is caused by a variation in the surface tension along a liquid−vapor surface.[1] As the surface tension is a *force* per unit length, where the "length" is parallel to the surface in a direction perpendicular to the gradient, this surface tension gradient creates liquid motion in the direction of higher surface tension. Surface tension gradients can be caused by (i) temperature gradients along the surface giving rise to the "thermal Marangoni effect" or by (ii) surface compositional gradients in binary liquid mixtures giving rise to the "solutal Marangoni effect". The thermal Marangoni effect causes liquid droplets[2] or wetting films[3] to move toward colder regions of a solid surface, as the surface tension increases with decreasing temperature. The solutal Marangoni effect is the cause for "tears of wine" observed on wine glasses[1,4] where a water−ethanol film climbs up the surface of the wine glass due to the preferential evaporation of the more volatile ethanol component at the leading edge of the film. Eventually, this climbing water−ethanol film undergoes a "Marangoni instability", at its leading edge, which gives rise to the "tears" of wine. The solutal Marangoni effect due to surface variations in composition can be caused by chemical reactions,[5] evaporation,[6] or dilatations and compressions of a surface layer.[7] A Marangoni instability is often associated with the Marangoni effect and may occur at the leading edge of an advancing film or within a thin liquid film. For example, if a temperature gradient is applied *perpendicular* to a liquid−vapor surface, the liquid−vapor surface becomes unstable above a critical Marangoni number where convection cells are generated whose size depends upon the size of the temperature gradient and the depth of the liquid film across which the temperature gradient is applied.

Of current interest is the ability to self-assemble nanoparticles (NPs), in solution, into two- and three-dimensional superlattice materials.[8] The solutal Marangoni effect has been used to self-assemble NP films onto solid silica surfaces from NP solutions.[9] The precise NP deposition mechanism onto a solid surface is complex and not well understood. In general, an aqueous and organic biphasic mixture is required where deposition only occurs after these two phases are vigorously mixed. In Mayya and Sastry,[9a] carboxylic acid derivatized 13 nm diameter gold NPs in an aqueous medium were vigorously mixed with an organic phase composed of toluene and the surfactant (or ligand) octadecylamine. In Johnson et al.,[9b] the aqueous phase consisted of water, ethanol, the surfactant (or ligand) 11-mercaptoundecanoic acid, and HCL, while the organic phase consisted of TAB (tetraoctylammonium bromide) ligated 5−8 nm diameter Ag NPs in chloroform. The NP film growth rate of ~0.1−1 cm/s depended sensitively upon solution conditions (e.g., surfactant concentration, aqueous medium pH, water/ethanol relative volume fraction, etc.). NP film growth required that the hydrophilic silica surface be prewetted by a water film. Ligand exchange between the surfactant ligand and the ligand, which initially surrounds the NP, may occur upon NP film deposition onto the silica surface. The Marangoni effect and Marangoni instability have also been used to self-assemble NPs into patterns on solid surfaces. In highly volatile solvents, such as hexane or chloroform, NP rings and honeycomb networks can be formed on a solid surface where the morphology depends upon the NP concentration in

Received: December 5, 2011
Revised: February 22, 2012
Published: February 23, 2012

   dx.doi.org/10.1021/jp211691q | *J. Phys. Chem. C* 2012, 116, 6052−6057

the solvent.[10] These patterns have been attributed to the Marangoni instability and dewetting dynamics of the solvent. More organized, complex NP patterns on solid surfaces, induced by the Marangoni effect, can be obtained by using multiple solvents and varying the wettability of the solid substrate relative to the solvents. On nonwettable substrates, Cai and Newby[11] observed circular NP rings arranged in a hexagonal pattern due to the simultaneous evaporation of ethanol and condensation of water (from wet N_2 gas). The ring size and inter-ring separation was controlled by varying the relative humidity of the N_2 gas. On wettable substrates, the ethanol evaporation combined with water condensation gave rise to a pattern of NP stripes. The formation of NP films and patterns on solid surfaces is poorly understood; these processes depend upon the wettability of the liquid solvent for the solid surface as well as the wettability and solubility of the nanoparticle for the liquid.

In this publication, we describe observations of a novel NP-enhanced Marangoni liquid transport in an NP–octadecane solution near the melting point of octadecane. The NPs used in these experiments consist of 5 nm diameter gold NPs coated with a dodecanethiol ligand, which are known to adsorb at the liquid–vapor surface of the octadecane solvent.[12] The essence of the Marangoni phenomenon that we observe is well represented by Figure 1. A thermal gradient is applied to a thin film of this NP–octadecane mixture situated in a shallow open Teflon trough. The temperature distribution is such that a solid–liquid boundary forms at the midpoint of this trough so that half of this mixture is frozen and the other half is liquid (Figure 2a). Over time, all of the liquid phase is transported via a Marangoni effect over to the solid phase where eventually it freezes. A solidified "mountain" builds up at the solid–liquid boundary (Figure 1) as a result of this liquid transportation. This effect is present even for pure octadecane. Small concentrations of NPs in the bulk octadecane solvent (NP volume fractions $\phi \sim 10^{-5}$) increase the rate of this Marangoni transportation process by up to a factor of 4 for the NP concentrations studied.

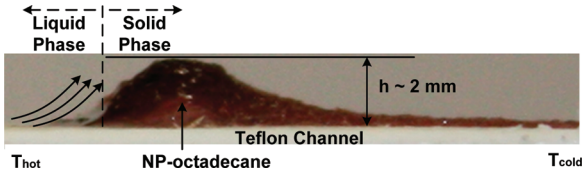

Figure 1. Side view of an ~2 mm high "mountain" generated at the liquid–solid boundary of a dodecanethiol ligated Au nanoparticle–octadecane mixture situated in a thermal gradient of 0.74 °C/cm, where half the mixture is liquid and the other half is solid. The nanoparticle concentration is 0.5 mg/mL. Thermal and solutal Marangoni liquid flow creates this mountain over a time period of 2 h.

2. EXPERIMENTAL METHODS

In order to quantitatively characterize this unusual Marangoni effect, we have used a digital camera to measure the mountain height h as well as the relative liquid flow volume ΔV as a function of both time and NP bulk concentration, as described in this section.

Materials. *n*-Octadecane (99+%) and anhydrous methanol (99.8%) were purchased from Sigma-Aldrich and used as received.

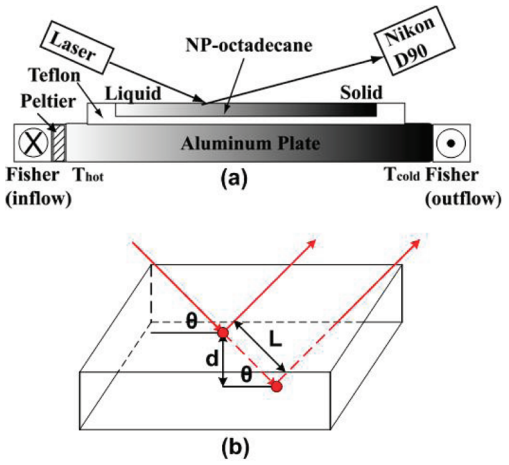

Figure 2. (a) Schematic of the experimental configuration used to study Marangoni flow near the melting point of the NP–octadecane mixture. A temperature gradient is applied to the aluminum plate via a Fisher Scientific (cold) water bath and a peltier heater. (b) Depiction of the reflected laser beam method for measuring the change in height d of the liquid–vapor surface.

Dodecanethiol-coated gold NPs (gold core diameter 5.0 ± 0.5 nm and ligand shell thickness 1.7 nm) were synthesized via a digestive ripening procedure.[13] The as-prepared gold NPs came dissolved in toluene. This toluene solvent was exchanged with *n*-octadecane by precipitating the gold NPs out of solution using methanol (2:1 methanol to toluene) at a centrifugation of 1050*g* for 15 min. The solid NP precipitate was dried using ultrahigh purity nitrogen gas and then redissolved in the *n*-octadecane solvent via stirring and sonication. Large clusters were removed via centrifugation at 14100*g* for 10 min at a temperature of $T \sim 30$ °C; the NP–octadecane supernatant was used in these experiments.

Concentration Measurements. The bulk NP concentration in *n*-octadecane solvent was determined from the solution absorbance[14] at the NP plasmon resonance wavelength of 523 nm using a CCD-array UV–vis spectrophotometer (Spectral Instruments, Inc.). Most samples were diluted before measurement in order to exclude errors arising from the turbidity of the solution.

Experimental Configuration. The melting temperature of pure *n*-octadecane as well as all of the NP–octadecane solutions exhibited a melting temperature of $T_m \approx 28$ °C. 400 μL of well-mixed premelted NP–octadecane solution, at the appropriate bulk NP concentration, was transferred to a warm (>30 °C) homemade Teflon channel (5.4 cm long (l) × 1.1 cm wide (w) × 0.5 mm deep) before solidification of this sample at ~20 °C. The Teflon channel maintains excellent thermal contact with an underlying aluminum plate (Figure 2a) via high thermal conductivity paste (Omegatherm 201). Uniform temperature distributions were applied to the aluminum plate using a Fisher Scientific water bath (ISOTEMP 1006D). A temperature gradient ($T_{hot} = 30.2 \pm 0.05$ °C, $T_{cold} = 26.2 \pm 0.05$ °C, $dT/dx = 0.74$ °C/cm) was applied along the length of the Teflon channel using a ceramic peltier heater (Laird Technologies, model CP10.30.05.L1W4.5) at one end of the aluminum plate and a cooling system consisting of the Fisher Scientific water bath at the other end. The peltier heater was maintained at a constant temperature using a Wavelength Electronics temperature controller (model LFI-3551). The temperature distribution along the Teflon channel was

dx.doi.org/10.1021/jp211691q | J. Phys. Chem. C 2012, 116, 6052–6057

monitored using a number of thermistors (Wavelength Electronics, model TCS650, 50 kΩ thermistor) and a digital multimeter (Keithley, model 197). For each sample, after application of the temperature gradient, 30 min was allowed for a steady-state temperature distribution to establish itself before commencing computer-controlled measurements (at specified times t) of the mountain height h and relative liquid flow volume ΔV using two digital cameras (Canon 450D and Nikon D90, respectively). $\Delta V = lwd/2$, where d is the depth of liquid *removed*, was measured by determining the *shift* in the position of a reflected 632 nm HeNe laser beam from the liquid–vapor surface onto the Nikon D90 digital camera (Figure 2b). The Nikon D90 measures the reflected beam shift distance L over some time period Δt; hence, the depth of liquid removed is $d = L \sin\theta$.

3. EXPERIMENTAL OBSERVATIONS

Figure 3 shows a time sequence of this Marangoni transportation process for a NP concentration of 0.25 mg/mL. At each time step, a top view and side view are shown where the ruler graduations have been carefully aligned so that a quantitative comparison can be made of features in the two different perspectives. The ruler numberings are in units of centimeters. Initially, a uniformly mixed ~0.5 mm thick NP–octadecane solution is solidified in the shallow Teflon trough (Figure 3a, t = 0 h). The NP–octadecane appears a uniform purplish color due to the plasmon resonance peak of the 5 nm diameter gold nanoparticles. The white opaque side walls of the Teflon trough block any observation of the NP–octadecane mixture in the side view. After 0.5 h of application of this gradient, the solid and liquid phases are clearly delineated (Figure 3b). The solid side of the trough is noticeably more purplish in color than the liquid side due to nanoparticle transportation. In agreement with normal (thermal) Marangoni transport, the liquid moves toward the colder portion of the container, a phenomenon which is present even for pure octadecane. The beginning of a mountain is just observable in the side view after 1 h (Figure 3c). The height of the mountain steadily increases with time (Figure 3d–f) until it is 2 mm high after 12 h (Figure 3f). At 2 h, the liquid has started to overflow the sides of the trough (Figure 3d, top view) where a white line (due to reflection from the room lights) is apparent at the Teflon–liquid–vapor contact line in Figure 3d and e. In the final frame (Figure 3f), after 12 h, this reflection has disappeared which is an indication that all of the liquid has now solidified. All of the liquid has now been removed from the liquid side of the trough so that it appears white in the top view. The 2 mm high "mountain" is clearly asymmetric with a gradient of ~45° on the "steeper" side of the mountain where it is apparent that the mountain commences building at the position of the liquid–solid boundary. The top view is noticeably more purplish in color where the mountain has built up due to the deposition of nanoparticles.

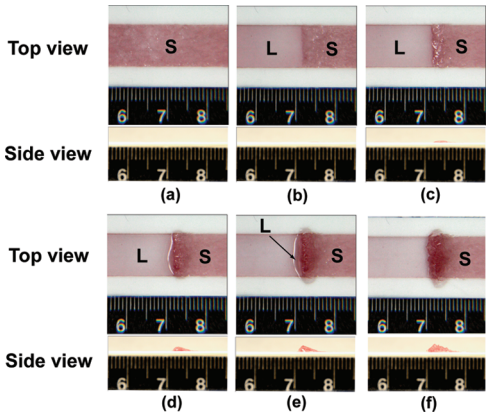

Figure 3. Top and side views of the mountain building process at the liquid (L)–solid (S) boundary for a nanoparticle concentration of 0.25 mg/mL at various times: (a) 0, (b) 0.5, (c) 1, (d) 2, (e) 4, and (f) 12 h. Ruler graduations (in units of cm), in the top and side views, have been carefully aligned so that phenomena in the two views can be directly compared. The melting of the liquid side, and its transfer to the solid side of the sample, is readily apparent in the top view. The growth of the mountain, above the Teflon trough, is readily apparent in the side view.

The variation in mountain height h with time, for various bulk concentrations of NPs, is shown in Figure 4a. As noted earlier, all data sets start at 0.5 h corresponding to the wait time for a steady-state temperature distribution to be attained. It is evident from this figure that the presence of NPs causes the mountain to grow faster. As a measure of the **early** mountain growth rate, we have plotted $\Delta h/\Delta t$ in Figure 5a, averaged over the time period 0.5–1.25 h. There is an initial rapid increase in growth rate at low NP concentrations from a value of ~0.4 mm/h, for pure octadecane, to ~0.65 mm/h at a NP bulk concentration of 0.01 mg/mL. The growth rate then plateaus at this growth rate value of ~0.65 mm/h out to a NP bulk concentration of ~0.15 mg/mL. Above this NP concentration of ~0.15 mg/mL, the mountain growth rate increases to ~1.6

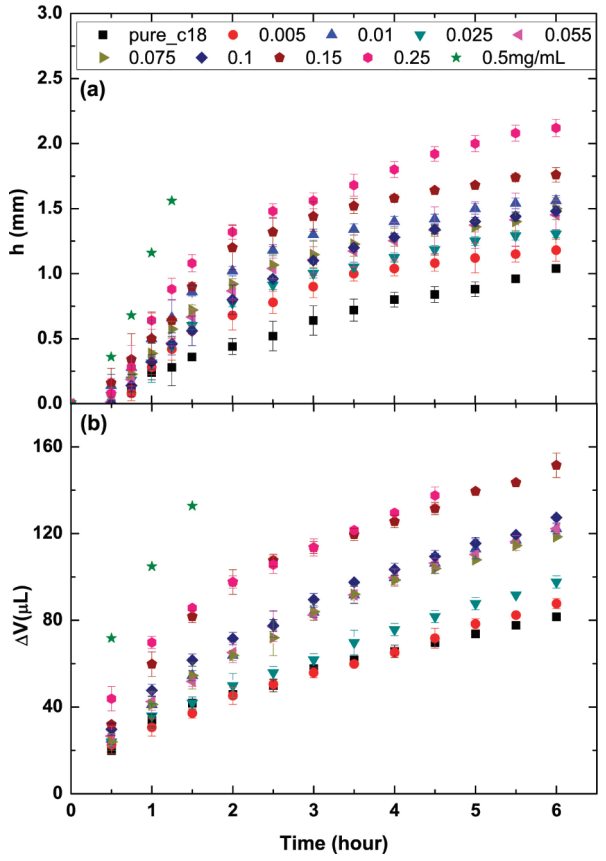

Figure 4. (a) Mountain height h and (b) total liquid flow volume ΔV versus time for various bulk NP concentrations.

dx.doi.org/10.1021/jp211691q | J. Phys. Chem. C 2012, 116, 6052–6057

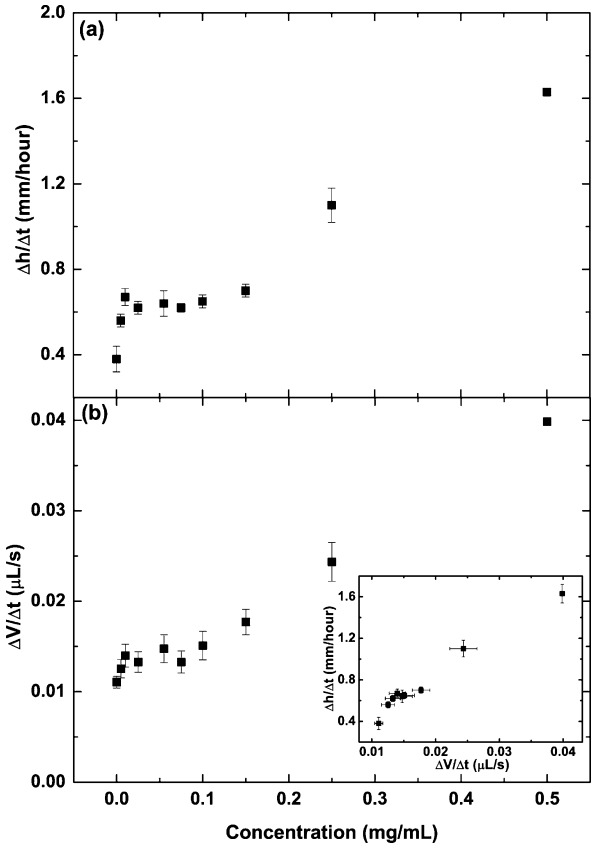

Figure 5. Early time (0.5−1 h) (a) mountain height change $\Delta h/\Delta t$ and (b) volume flow rate $\Delta V/\Delta t$ as a function of bulk NP concentration determined from Figure 4. (Inset) $\Delta V/\Delta t$ versus $\Delta h/\Delta t$ derived from parts a and b.

mm/h at the highest NP concentration studied (0.5 mg/mL), which is 4 times the growth rate of pure octadecane studied under identical thermal conditions.

Figure 4b shows the total liquid volume change ΔV due to Marangoni flow measured as a function of time for various NP concentrations. As in the measurement of h (Figure 4a), 0.5 h was allowed for a steady-state temperature distribution to be attained. Note that, as only *relative* volume changes can be determined, from the beam shift (rather than absolute volumes), the first sequence of points at time t = 0.5 h for various NP concentrations measures the change in volume ΔV from times t = 0.5 to 1.0 h. As expected, parts a and b of Figure 4 exhibit remarkably similar behavior where both figures indicate that the presence of NPs significantly increases the Marangoni flow. For example, at a time of 6 h, the mountain height of the 0.15 mg/mL sample is a factor of 1.8 times larger than the pure octadecane sample (Figure 4a). For comparison, at 6 h, the total liquid volume flow of the 0.15 mg/mL sample is a factor of 1.9 times larger compared with the pure octadecane sample (Figure 4b). In Figure 5b, we show the volume flow rate $\Delta V/\Delta t$ as a function of NP concentration at early times, calculated from the first sequence of points in Figure 4b at t = 0.5 h where, as stated earlier, Δt = 0.5 h for these sequence of measurements. Figure 5b exhibits similar behavior to Figure 5a. There is an increase in the volume flow rate for low NP concentrations up to 0.01 mg/mL. This volume flow rate then exhibits a plateau and remains constant up to an NP concentration of ∼0.1 mg/mL. Above this concentration, the volume flow rate then increases up to the highest NP concentration studied of 0.5 mg/mL. The volume flow rate at the highest NP concentration of 0.5 mg/mL is a factor of 3.6 times larger than the pure octadecane system. This behavior is similar to the factor of 4 observed in Figure 5a in comparing the mountain growth rate for the highest NP concentration to the pure system. The volume flow rate $\Delta V/\Delta t$ is obviously the cause for the mountain growth rate $\Delta h/\Delta t$. The Figure 5b inset demonstrates that $\Delta h/\Delta t$ is approximately linearly proportional to $\Delta V/\Delta t$.

4. DISCUSSION

The behavior exhibited in Figures 4 and 5 is obviously complex. The presence of nanoparticles clearly enhances the flow of liquid toward the colder solidified regions of the NP−octadecane sample. A thermal gradient also induces motion of particles in the bulk liquid, the Soret effect.[15] De Gennes[16] argues that Soret flow (just below the liquid−vapor surface) is negligible in comparison with Marangoni flow induced by the presence of a surface tension gradient. He argues that the ratio of these two flows is proportional to a molecular length divided by the liquid film thickness; hence, in this discussion we will neglect any liquid motion induced by the Soret effect.

Marangoni flow is caused by a difference in surface tension $\Delta\gamma$ along the liquid−vapor surface. This difference in surface tension can be induced either by a difference in temperature or by a difference in surface composition along the surface. In order to understand these two contributions to Marangoni flow, it is therefore important to know how the surface tension γ changes with temperature and NP bulk composition, respectively. Figure 6 shows the *equilibrium* NP−octadecane

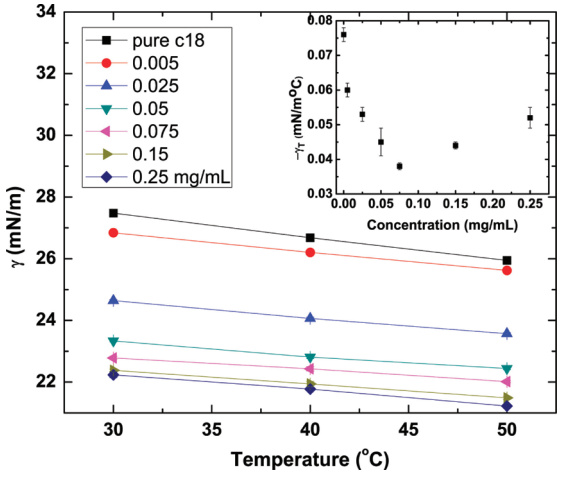

Figure 6. Equilibrium surface tension γ versus temperature for various bulk NP concentrations. Inset: surface tension dependence $\gamma_T = d\gamma/dT$ versus bulk NP concentration.

surface tension measured as a function of temperature for various NP bulk compositions determined via the pendant drop technique after waiting an equilibrium time of 30 min at each temperature.[12] The temperature dependence $\gamma_T = d\gamma/dT \sim -0.05$ mN/m °C is similar for all NP−octadecane solutions. Figure 7 shows the *equilibrium* NP−octadecane surface tension plotted as a function of bulk NP concentration measured at a constant temperature of 30 °C.[12] According to a statistical mechanics based theory,[12] dodecanethiol ligated Au NPs in octadecane solvent are strongly surface active with a NP surface volume fraction of $\phi_s \sim 0.1-0.8$, depending upon the NP bulk

dx.doi.org/10.1021/jp211691q | J. Phys. Chem. C 2012, 116, 6052−6057

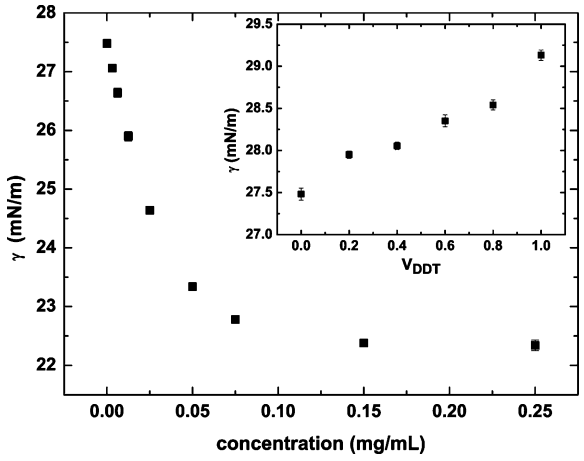

Figure 7. Equilibrium surface tension γ versus bulk NP concentration for dodecanethiol ligated Au nanoparticles in *n*-octadecane solvent measured at a temperature of 30 °C.[12] Inset: octadecane + dedecanethiol surface tension at 30 °C as a function of dedecanethiol volume fraction.

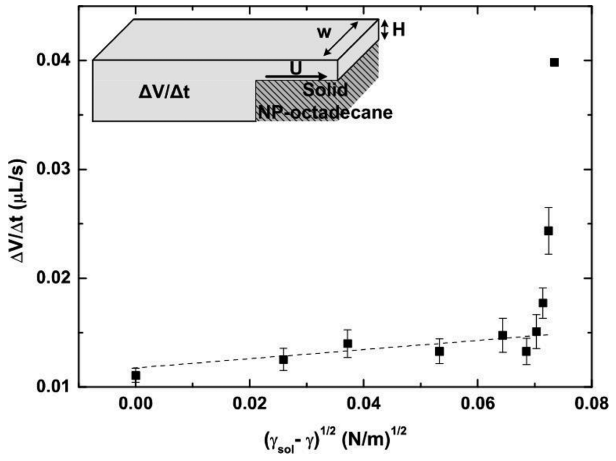

Figure 8. $\Delta V/\Delta t$ versus $(\gamma_{sol} - \gamma)^{1/2}$, experimental data (symbols) and eq 6 (dashed line) with $C_1 = 1.2 \times 10^{-11}$ m^3/s and $C_2 = 3.1 \times 10^{-11}$ m$^{7/2}$/(s N$^{1/2}$), where $A \sim 0.03$ nm/s. (Inset) Simplified geometry used to model the rate of liquid flow $\Delta V/\Delta t$ through a liquid channel of height H and width w (on top of a solidified NP–octadecane mixture) at a liquid velocity U.

volume fraction in the range $\phi \sim 10^{-6}$–10^{-5}. This strong NP surface activity originates from the fact that NP adsorption at the liquid–vapor surface of octadecane considerably lowers the NP–octadecane solution surface energy. Specifically, the NP surface energy is $\gamma_{NP} = 20.9$ mN/m (determined by the methyl terminal group ($-CH_3$) of the ligand coating surrounding the NP[12]), while the octadecane surface tension is $\gamma_{C18} = 27.5$ mN/m; hence, it is energetically favorable for the NP to adsorb at the liquid–vapor surface of the NP–octadecane solution. Note that the surface tension decrease with increasing NP concentration, observed in Figure 7, cannot be explained by the adsorption of residual dodecanethiol ligands that may be present in solution. The Figure 7 inset plots the surface tension of an octadecane + dodecanethiol mixture as a function of the dodecanethiol volume fraction; consequently, the adsorption of any residual dodecanethiol ligands would tend to increase the NP-solution surface tension.

To obtain a quantitative understanding of Figures 4 and 5 is difficult. In this section, we compare currently available theory with the *early time* steady-state volume flow behavior and how it depends upon bulk NP concentration (Figure 5b). As a temperature difference of only 4 °C is applied along the 5.4 cm length of the Teflon trough, it is readily apparent from Figure 6 that the surface tension difference induced by this temperature difference is $\Delta\gamma < 0.5$ mN/m and that the magnitude of this thermal Marangoni contribution will be similar, independent of the NP bulk concentration, because $d\gamma/dT$ is similar for all NP concentrations. By contrast, if a surface concentration gradient in the NPs can be created, then the solutal Marangoni effect could be much larger as, in this case, $\Delta\gamma \sim 5$ mN/m (Figure 7).

In order to qualitatively explain certain aspects of Figure 5b, we use an extremely simple model that captures many of the essential physical features. The liquid volume flow $\Delta V/\Delta t$ is modeled as flowing through a thin horizontal channel of height H and width w at velocity U on top of the solidified solution (Figure 8, inset). Gravitational effects have been ignored in this simplified model. Volume conservation requires that

$$\frac{\Delta V}{\Delta t} = HwU = Hw(U_T + U_\phi) \tag{1}$$

where the velocity U is composed of two components U_T and U_ϕ due, respectively, to a thermal and surface composition gradient. We have assumed additivity of these two velocities. In flowing through this thin channel, the velocity will be slowed by viscosity η effects where the velocity due to a temperature gradient[3]

$$U_T = -\frac{H}{2\eta}\frac{d\gamma}{dT}\frac{dT}{dx} \tag{2}$$

and that due to a surface composition gradient[6a]

$$U_\phi = -\frac{H}{2\eta}\frac{d\gamma}{d\phi}\frac{d\phi}{dx} \tag{3}$$

where ϕ is the NP volume fraction. For our geometry, $w = 1.1$ cm, $dT/dx = 0.74$ °C/cm, $d\gamma/dT \approx -0.05$ mN(m °C) (Figure 6), and $\eta = 0.0035$ kg/(m s); therefore, from the pure octadecane $\Delta V/\Delta t$ value and eqs 1 and 2, one finds a film thickness $H \approx 43$ μm and thermal velocity flow $U_T \approx 23$ μm/s. As there seems to be little compelling reason for H to vary significantly due to the presence of small concentrations of NPs, the thermal velocity U_T is expected to be constant independent of NP concentration, as neither η nor $d\gamma/dT$ vary significantly with ϕ.

Figure 4b requires that the solutal Marangoni velocity (U_ϕ) be in the same direction as the thermal Marangoni velocity (U_T), as the liquid volume change ΔV increases with increasing NP concentration over and above that observed for pure octadecane. U_T is caused by a higher surface tension at lower temperatures. For U_ϕ to be in the same direction as U_T therefore, according to Figure 7, the NP liquid–vapor surface concentration in the thin liquid channel (above the solidified NP–octadecane mixture) must be less than the corresponding NP surface concentration above the bulk liquid solution. Within the thin liquid channel, we believe that the NPs freeze out of solution faster than the octadecane itself solidifies and that this is the physical mechanism that creates the solutal Marangoni effect (or, perhaps, equivalently at lower temperatures the solubility of the NPs in octadecane is lower and some of the NPs phase separate out of solution within the thin film). Here, we adapt a theory due to de Ryck[6a,17] to explain solutal

dx.doi.org/10.1021/jp211691q | J. Phys. Chem. C 2012, 116, 6052–6057

Marangoni flow. This theory was originally designed to explain solutal Marangoni flow in binary liquid thin films (e.g., water−ethanol mixtures) where due to evaporation of the more volatile component (ethanol) a surface composition gradient was created which leads to a solutal Marangoni flow (the "tears of wine" effect in a glass of wine). According to de Ryck[6a,17]

$$U_\phi = \sqrt{-\frac{A\phi(1-\phi)}{2\eta}\frac{d\gamma}{d\phi}} \tag{4}$$

where, for our situation, A (>0) represents the freezing velocity of the NPs. As

$$\phi\frac{d\gamma}{d\phi} \approx \phi\frac{\Delta\gamma}{\Delta\phi} = \gamma - \gamma_{sol} \tag{5}$$

where γ (γ_{sol}) is the NP-solution (pure octadecane) surface tension, hence, from eqs 1, 4, and 5

$$\frac{\Delta V}{\Delta t} = C_1 + C_2\sqrt{\gamma_{sol} - \gamma} \tag{6}$$

with constants

$$C_1 = HwU_T \tag{7}$$

and

$$C_2 \approx Hw\sqrt{\frac{A}{2\eta}} \tag{8}$$

Figure 8 shows a plot of $\Delta V/\Delta t$ versus $(\gamma_{sol} - \gamma)^{1/2}$. For low NP concentrations up to 0.1 mg/mL, eq 6 provides a reasonable description of the observed trend for a freezing velocity of $A \sim 0.03$ nm/s. At higher NP concentrations, significant deviations from eq 6 are observed, and in this case, $\Delta V/\Delta t$ appears to vary linearly with ϕ (Figure 5b). The "kink" in Figure 8 at $(\gamma_{sol} - \gamma)^{1/2} \sim 0.07(N/m)^{1/2}$ is caused by the fact that γ saturates for NP concentrations above ∼0.1 mg/mL (Figure 7). At higher NP concentrations above 0.1 mg/mL, some other mechanism, not accounted for by eq 4, must play a role. It remains to be seen whether or not a more sophisticated analysis based upon a solution of the continuity and Stokes equations,[18] with appropriate boundary conditions, can provide a more comprehensive explanation of the results in Figures 4 and 5.

5. SUMMARY

In this publication, we document NP-enhanced Marangoni transport in a NP−octadecane solution near the freezing point of this mixture. A thermal gradient is applied to a thin film of this mixture in an open Teflon trough such that the liquid−solid boundary forms approximately in the middle of the Teflon trough and where half the mixture is frozen and the other half is liquid. Over a period of many hours, the NP−octadecane liquid flows in the direction of the solidified mixture where it forms a mountain of frozen material at the liquid−solid boundary (Figures 1 and 3). The mountain height h (Figure 4a) and liquid flow volume ΔV (Figure 4b) are measured as a function of time and NP bulk concentration. Small concentrations of NPs (bulk NP volume fractions $\sim 10^{-6}$−10^{-5}) considerably enhance the rate at which the mountain is built (Figure 5a), as well as the rate at which liquid flows (Figure 5b) in the direction of the solidified sample. NPs are known to adsorb strongly at the liquid−vapor surface of this NP−octadecane mixture. We believe that this NP-enhanced flow is due to the preferential freezing out of the NPs in the Marangoni flow relative to the solidification of octadecane, thus creating a NP concentration gradient at the liquid−vapor surface which leads to a strong solutal Marangoni flow. A simple model of this NP freezing process (eqs 6−8) provides a description of the liquid volume flow rate $\Delta V/\Delta t$ as a function of bulk NP concentration at least for bulk NP concentrations less than ∼0.1 mg/mL (Figure 8). This simple model cannot explain the enhanced Marangoni flow at still higher bulk NP concentrations.

AUTHOR INFORMATION

Corresponding Author

*E-mail: bmlaw@phys.ksu.edu.

Notes

The authors declare no competing financial interest.

ACKNOWLEDGMENTS

The authors wish to thank members of the NSF NIRT collaboration for useful comments. This research was conducted with support from the US National Science Foundation under grants DMR-0603144 and CTS-0609318.

REFERENCES

(1) Scriven, L. E.; Sternling, C. V. *Nature* **1960**, *187*, 186.
(2) (a) Brochard, F. *Langmuir* **1989**, *5*, 432. (b) Brzoska, J. B.; Brochard-Wyart, F.; Rondelez, F. *Langmuir* **1993**, *9*, 2220.
(3) Schneemilch, M.; Cazabat, A. M. *Langmuir* **2000**, *16*, 8796.
(4) De Gennes, P.-G.; Brochard-Wyart, F.; Quere, D. *Capillarity and wetting phenomena*; Springer-Verlag: New York, 2004.
(5) (a) Vedove, W. D.; Sanfeld, A. *J. Colloid Interface Sci.* **1981**, *84*, 318. (b) Kozhoukharova, Z. D.; Slavchev, S. G. *J. Colloid Interface Sci.* **1992**, *148*, 42.
(6) (a) Fanton, X.; Cazabat, A. M. *Langmuir* **1998**, *14*, 2554. (b) Guena, G.; Poulard, C.; Cazabat, A. M. *Colloids Surf., A* **2007**, *298*, 2.
(7) Sorensen, T. S. *Lecture Notes in Physics*; Springer-Verlag: Berlin, 1979; Vol. *105*.
(8) (a) Bigioni, T. P.; Lin, X.-M.; Nguyen, T. T.; Corwin, E. I.; Witten, T. A.; Jaeger, H. M. *Nat. Mater.* **2006**, *5*, 265−270. (b) Prasad, B. L. V.; Sorensen, C. M.; Klabunde, K. J. *Chem. Soc. Rev.* **2008**, *37*, 1871.
(9) (a) Mayya, K. S.; Sastry, M. *Langmuir* **1999**, *15*, 1902. (b) Johnson, D. D.; Kang, B.; Vigorita, J. L.; Amram, A.; Spain, E. M. *J. Phys. Chem. A* **2008**, *112*, 9318.
(10) (a) Maillard, M.; Motte, L.; Ngo, A. T.; Pileni, M. P. *J. Phys. Chem. B* **2000**, *104*, 11871. (b) Stowell, C.; Korgel, B. A. *Nano Lett.* **2001**, *1*, 595.
(11) Cai, Y.; Newby, B. Z. *J. Am. Chem. Soc.* **2008**, *130*, 6076.
(12) Wi, H. S.; Cingarapu, S.; Klabunde, K.; Law, B. M. *Langmuir* **2011**, *27*, 9979.
(13) (a) Lin, X.-M.; Sorensen, C. M.; Klabunde, K. J. *J. Nanopart. Res.* **2000**, *2*, 157. (b) Prasad, B. L. V.; Stoeva, S. I.; Sorensen, C. M.; Klabunde, K. J. *Langmuir* **2002**, *18*, 7515.
(14) Haiss, W.; Thanh, N. T. K.; Aveyard, J.; Femig, D. G. *Anal. Chem.* **2007**, *79*, 4215−4221.
(15) de Groot, S.; Mazur, P. *Nonequilibrium thermodynamics*; North-Holland: Amsterdam, The Netherlands, 1962.
(16) De Gennes, P.-G. *C. R. Acad. Sci.* **1982**, 295.
(17) de Ryck, A. *J. Colloid Interface Sci.* **1999**, *209*, 10.
(18) (a) Hu, H.; Larson, R. G. *Langmuir* **2005**, *21*, 3963. (b) Hu, H.; Larson, R. G. *Langmuir* **2005**, *21*, 3972.